Bone Reports 7 (2017) 63–69

Contents lists available at ScienceDirect

Bone Reports

journal homepage: www.elsevier.com/locate/bonr

Case Report

MicroRNA expression in a phosphaturic mesenchymal tumour

Darrell Green[a], Irina Mohorianu[b], Isabelle Piec[a], Jeremy Turner[c], Clare Beadsmoore[d], Andoni Toms[d], Richard Ball[e], John Nolan[f], Iain McNamara[f], Tamas Dalmay[b], William D. Fraser[a,c,g,*]

[a] Norwich Medical School, University of East Anglia, Norwich Research Park, Norwich NR4 7TJ, United Kingdom
[b] School of Biological Sciences, University of East Anglia, Norwich Research Park, Norwich NR4 7TJ, United Kingdom
[c] Department of Diabetes and Endocrinology, Norfolk and Norwich University Hospital, Norwich Research Park, NR4 7UY, United Kingdom
[d] Norwich Radiology Academy, Norfolk and Norwich University Hospital, Norwich Research Park, NR4 7UB, United Kingdom
[e] Norfolk and Waveney Cellular Pathology Service, Norfolk and Norwich University Hospital, Norwich Research Park, NR4 7UB, United Kingdom
[f] Department of Orthopaedics and Trauma, Norfolk and Norwich University Hospital, Norwich Research Park, NR4 7UY, United Kingdom
[g] Department of Clinical Biochemistry, Norfolk and Norwich University Hospital, Norwich Research Park, NR4 7UY, United Kingdom

ARTICLE INFO

Keywords:
FGF23
Hypophosphatemia
Tumour
microRNA
Next generation sequencing

ABSTRACT

Phosphaturic mesenchymal tumours are a heterogeneous set of bone and soft tissue neoplasms that can cause a number of paraneoplastic syndromes such as tumour induced osteomalacia. The term phosphaturic comes from the common finding that these tumours secrete high levels of fibroblast growth factor 23 which causes renal phosphate wasting leading to hypophosphatemia. Phosphaturic mesenchymal tumours are rare and diagnosis is difficult. A very active 68 year old male presented with bone pain and muscle weakness. He was hypophosphataemic and total alkaline phosphatase was markedly elevated. The patient was placed on vitamin D supplementation but his condition progressed. In the fifth year of presentation the patient required the use of a wheelchair and described “explosive” bone pain on physical contact. Serum 1,25 dihydroxyvitamin D was low and serum fibroblast growth factor 23 was significantly elevated, raising suspicion of a phosphaturic mesenchymal tumour. A lesion was detected in his left femoral head and the patient underwent a total hip replacement. The patient displayed a rapid improvement to his condition and during a three year follow up period he returned to an active lifestyle. As molecular testing may help provide a robust diagnosis and is particularly useful in rare diseases we took a next generation sequencing approach to identify a differential expression of small RNAs in the resected tumour. Small RNAs are non-coding RNA molecules that play a key role in regulation of gene expression and can be used as specific biomarkers. We found an upregulation of miR-197. We also found a downregulation of miR-20b, miR-144 and miR-335 which is a small RNA profile typical of osteosarcoma. MiR-21, the most frequently upregulated microRNA in cancer, was downregulated. We conclude that the specific small RNA profile is typical of osteosarcoma except for the downregulation of oncogenic miR-21. Transcriptional plasticity of miR-197, which is computationally predicted to target fibroblast growth factor 23 messenger RNA, may be upregulated in a cellular effort to correct the ectopic expression of the protein.

1. Introduction

Fibroblast growth factor 23 (FGF23) interacts with the fibroblast growth factor receptor 1-klotho (FGFR1-KL) complex in renal tubules. The FGF23-FGFR1-KL interaction negatively regulates phosphate reuptake (Berndt and Kumar, 2007). Abnormally high circulating blood concentrations of FGF23 can be caused by ectopic secretion from phosphaturic mesenchymal tumours (PMTs) resulting in phosphate wasting and hypophosphatemia. Hypophosphatemia leads to decreased mineralisation of the bones and can contribute to tumour induced osteomalacia (TIO). FGF23 also blocks the expression of cytochrome P450 family 27 subfamily B member 1 (CYP27B1) which prevents the conversion of 25 hydroxyvitamin D (25(OH)D) to 1,25 dihydroxyvitamin D ($1,25(OH)_2D$). Low $1,25(OH)_2D$ reduces osteoid mineralisation (Chong et al., 2011). PMTs are typically low grade and require a step-wise approach to investigation utilising imaging and sometimes selective venous sampling for measurement of FGF23 to locate the lesion (Chong et al., 2011).

There have been few molecular studies of PMT that delineate understanding of their development and ectopic expression of FGF23

* Corresponding author at: Norwich Medical School, University of East Anglia, Norwich Research Park, Norwich NR4 7TJ, United Kingdom.
E-mail address: W.Fraser@uea.ac.uk (W.D. Fraser).

http://dx.doi.org/10.1016/j.bonr.2017.09.001
Received 2 June 2017; Received in revised form 31 August 2017; Accepted 4 September 2017
Available online 06 September 2017

causing paraneoplastic syndromes. The existing studies observe fibronectin 1 (FN1)-FGFR1 fusion genes in 60% of PMTs causing TIO (Lee et al., 2015). Unlike prototypical leukemia inducing FGFR1 fusions, which are ligand independent, the FN1-FGFR1 chimeric protein preserves its binding domains for FGF23 (Lee et al., 2015). Hypoxia inducible factor 1 alpha (HIF1A) has been observed to induce ectopic expression of FGF23 (Zhang et al., 2016). Hypoxia is a known driver of tumourigenesis by reducing the activity of oxygen dependent Tet methylcytosine dioxygenases (TETs) which are required for DNA demethylation of tumour suppressor genes (Thienpont et al., 2016).

We report a patient who presented with clinical and biochemical signs of TIO and in whom radiological appearances were consistent with renal osteodystrophy despite good renal function. Further investigation identified the presence of a PMT. Surgical resection of the tumour relieved the symptoms and corrected the biochemical abnormalities.

2. Case report

A 68 year old man had been in excellent health working as a farmer and performing manual labour until he presented with back pain and lower limb weakness. At presentation, magnetic resonance imaging (MRI) of the spine revealed a diffuse punctate reduction in signal on both T1 and T2 weighted sequences interspersed with areas of normal marrow fat signal. Conventional radiographs demonstrated poorly defined coarse trabeculae in the femoral necks that were characteristic of osteomalacia (Fig. 1A). There were periosteal reactions in the proximal tibia and patchy sclerosis in the proximal humerus and distal tibia (Fig. 1B). Serum biochemistry analysis using the Architect 8000 (Abbott, Maidenhead, UK) revealed the patient was hypophosphataemic with phosphate at 0.4 mmol/L (reference range 0.8–1.5 mmol/L) and total alkaline phosphatase was elevated at 400 U/L (reference range 38–126 U/L) (Fig. 2A and B). The patient was prescribed with 500 mg of calcium and 400 IU of vitamin D_3 per day but showed no improvement. He remained hypophosphataemic for the next five years.

In the fifth year since presentation the patient described “explosive” bone pain on physical contact. He now required the use of a wheelchair because of severe muscle weakness. Serum phosphate was now 0.52 mmol/L (reference range 0.8–1.5 mmol/L) and total alkaline phosphatase was now 213 U/L (reference range 38–126 U/L). Serum $1,25(OH)_2D$ (Radioimmunoassay, IDS, Boldon Colliery, UK) was 31 pmol/L (reference range 43–143 pmol/L) and C-Terminal FGF23 (Immutopics, Athens, USA) was 438 RU/mL (reference range < 100 RU/mL) (Fig. 2C and D). Liquid chromatography tandem mass spectrometry (LC-MS/MS) after protein precipitation detected 25 hydroxyvitamin D (25(OH)D) at 76 nmol/L (reference range 50–120 nmol/L). Adjusted calcium (Cobas® 6000, Roche, Burgess Hill, UK) was 2.4 mmol/L (reference range 2.1–2.6 mmol/L), creatinine (Cobas® 6000, Roche, Burgess Hill, UK) was 88 μmol/L (reference range 55–125 μmol/L) and intact parathyroid hormone (Cobas® 6000, Roche, Burgess Hill, UK) was 5.2 pmol/L (reference range 1.6–6.9 pmol/L). These fifth year investigations are summarised in Table 1 and were suggestive of a paraneoplastic syndrome. The patient was placed on vitamin D_3 supplementation at 20,000 IU per week for three months followed by 1000 IU per day for nine months. The patient was referred for radiography, bone densitometry, co-registered positron emission tomography/computerised tomography (PET/CT) and octreotide scintigraphy.

Dual-energy X-ray absorptiometry (DXA) revealed bone mineral density (BMD) in the lumbar spine was 1.498 g/cm^2 with a T-score of 3.7. BMD in the left femoral neck was 1.274 g/cm^2 with a T-score of 1.6. A radionuclide bone scintigram demonstrated multifocal radiotracer uptake in keeping with extensive insufficiency fractures involving the humeri, ribs, left glenoid, sacrum, left proximal femur and tibiae (Fig. 1C). CT of the chest, abdomen and pelvis revealed extensive sclerosis of the axial skeleton. Corresponding to an area of focal uptake in the left femoral head the CT demonstrated a well-defined lesion of the same attenuation as adjacent marrow and demarcated by a thin sclerotic rim (Fig. 1D). Pelvic and spinal sclerosis had increased since original presentation (Fig. 1E). PET/CT with ^{18}Fludeoxyglucose showed focal tracer accumulation in the left femoral head corresponding to a lucent lesion surrounded by sclerosis (Fig. 1F). There was new diffuse sclerosis evident throughout the pelvis and lumbar spine. The combination of osteosclerosis and osteomalacia suggested a radiological diagnosis of renal osteodystrophy but this was not supported by the normal renal function.

A decalcified one centimetre trephine bone biopsy of the lesion detected in the left femoral head showed trabecular thickening with increased woven and lamellar bone (Fig. 1G). The trabeculae had undulating surfaces suggesting previous remodelling activity. Osteoid, osteoblasts and osteoclasts were not conspicuous (Fig. 1G). Many trabeculae had a variable and thin zone of faintly basophilic staining at the surface possibly representing mineralised osteoid, though this observation is limited due to the decalcification method. The marrow contained an abnormal cellular infiltrate of variable density. Some areas were loosely cellular but others were more crowded and contained numerous overlapping hyperchromatic nuclei. Some nuclei showed streaming, other nuclei were palisaded. Nuclei were oval or grain shaped and had finely granular chromatin (Fig. 1G). Mitoses were rare. The cytoplasm was sparse and ill-defined. Cells were strongly immunoreactive for vimentin, CD56 and CD99. Cells did not stain for cytokeratins, smooth muscle actin, desmin, S100 protein, CD31, CD34, or CD117. There was a rich background capillary network (CD31, CD34) with interlinking branching vessels. Stromal calcification was present in small quantities. There was no necrosis. These observations were compatible with those described in PMT (Goldblum et al., 2013).

The confirmed tumour was resected by total hip replacement. The specimen was received immediately from theatre allowing fresh samples to be taken for molecular studies. After fixing in 10% formal saline, decalcification and routine processing to paraffin wax blocks, histopathological examination showed features similar to those in the biopsy. The neoplasm was composed of spindle shaped cells and had an infiltrative growth pattern. The lesion periphery appeared generally looser than the centre which was more compact and densely cellular. In places the tumour invested small arteries like a sleeve and appeared to infiltrate their media. Sections of formalin fixed paraffin embedded tumour specimen were incubated with an anti-FGF23 monoclonal antibody (AdipoGen, Liestal, Switzerland) for 24 h at ambient temperature after paraffin removal, rehydration and antigen retrieval using boiling EDTA (1 mM, pH 8). Endogenous peroxidase activity was inhibited by treatment with 3% hydrogen peroxide for 10 min at ambient temperature. The sections were then incubated with a 1:1000 horseradish peroxidase labelled secondary antibody (Abcam, Cambridge, UK) for 1 h at ambient temperature. Diaminobenzidine solution was used for visualisation followed by nuclear counterstaining with haematoxylin. Specificity of the FGF23 staining was determined by staining a serial section of the specimen using the same protocol with an isotope control antibody at the same concentration (Fig. 1H). The PMT section containing the anti-FGF23 monoclonal antibody showed positive staining for FGF23 (Fig. 1I).

During a three year follow up period since surgery the patient reported a rapid improvement of his condition and serum biochemistry normalised (Fig. 2A–D). He no longer required a wheelchair, was working again on his farm and performing heavy manual labour.

To the best of our knowledge a PMT associated with osteosclerosis has not previously been described. To gain molecular insight we took a next generation sequencing approach to investigate the small RNA population in the tumour. Small RNAs are non-coding RNA molecules that are key regulators of gene expression by negatively regulating target messenger RNAs (Green et al., 2016). Small RNAs such as microRNAs (miRNAs) can potentially be used to classify poorly differentiated tumours, distinguish between different subtypes of tumour

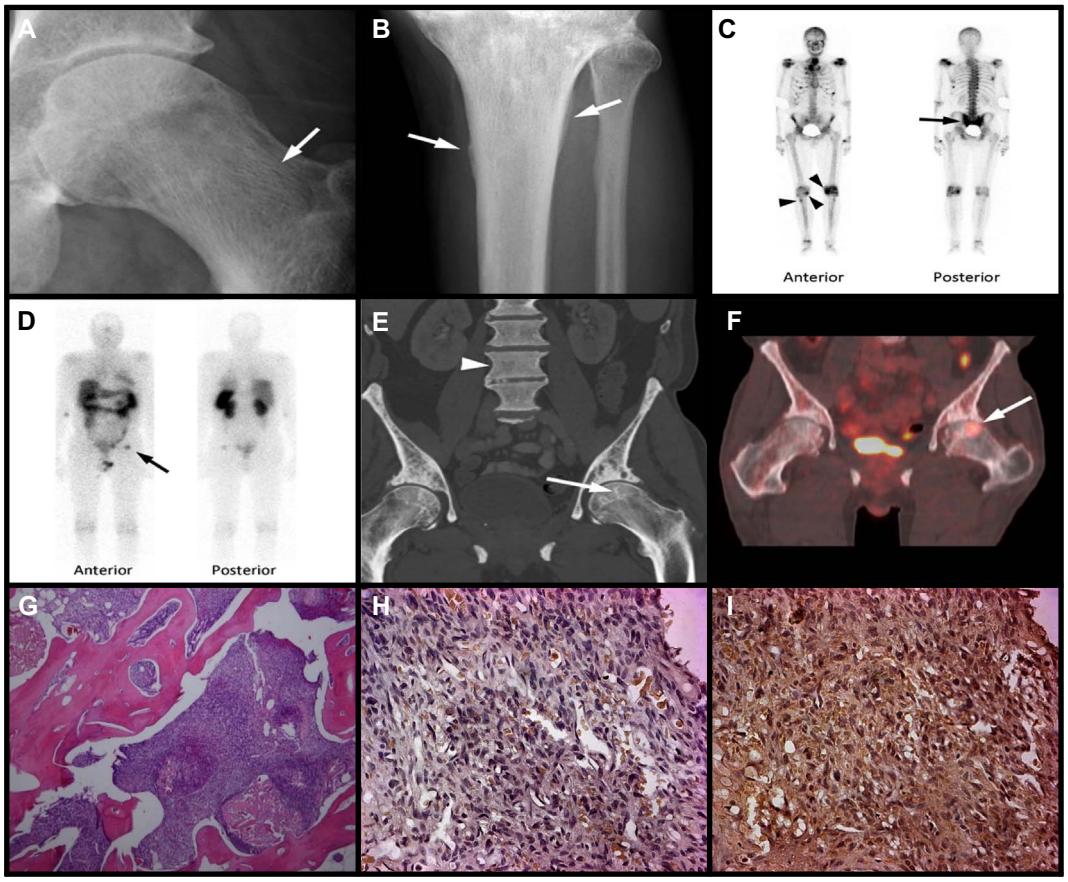

Fig. 1. The clinical course of a patient who presented with bone pain and muscle weakness. (A) Anteroposterior radiographs of the left femoral head and neck, demonstrating the typical but often subtle features of conventional osteomalacia with coarse ill-defined secondary trabeculae (arrow). (B) Anteroposterior radiograph of the right tibia demonstrating medial and lateral periosteal reactions along the proximal metaphysis (arrows). (C) Radionuclide bone scintigram demonstrating "H" shaped radiotracer uptake in the sacrum (arrow) with smaller foci of radiotracer uptake in the proximal tibiae (arrowheads). Proximal humeri, left glenoid, left lesser trochanter, right distal tibia and multiple ribs display focal, oft linear tracer accumulation in keeping with insufficiency fractures. (D) Anterior and posterior late phase images from on octreotide radionuclide examination demonstrating radiotracer uptake (arrow) in the left femoral head. (E) A coronal reformatted CT of the pelvis demonstrates a lesion in the left femoral head of the same attenuation as the surrounding medulla but demarcated by a thin sclerotic margin (arrow). There is diffuse medullary sclerosis throughout the lumbar spine (arrowhead). (F) Coronal fused ^{18}Fluorodeoxyglucose demonstrating increased tracer uptake in the lesion. (G) Photomicrograph at 20 × magnification of the lesion biopsy stained with haematoxylin and eosin. There is irregularly thickened trabecular bone with intervening densely cellular tumour. (H) Photomicrograph at 40 × magnification of anti-FGF23 negative control. (I) Photomicrograph at 40 × magnification of anti-FGF23 positive staining.

originating from the same tissue and as biomarkers in various biofluids (Rosenfeld et al., 2008; Yanaihara et al., 2006; Schetter et al., 2008; Blondal et al., 2013). Small RNA library construction and next generation sequencing is biased. If there is low complementarity between the adapter and small RNA the two molecules are less likely to be annealed and amplified. Small RNAs that are less likely to anneal to adapters are less likely to be sequenced. We previously developed high definition (HD) adapters which contain four degenerate assigned nucleotides on each of the ligating ends of HiSeq 2500 adapters (Sorefan et al., 2012; Xu et al., 2015). HD adapters increase annealing efficiency, reduce ligation bias and recover more small RNA sequences for analysis (Xu et al., 2015). We used HD adapters to identify differential expression of miRNAs in the PMT when compared to controls.

3. Materials and methods

3.1. Ethics for non-clinical procedures

This study was approved by the Faculty of Medicine and Health Sciences Research Ethics Committee. Clinical material was obtained from the Norwich Biorepository which collected bone tissue from the Norfolk and Norwich University Hospital. The patient and control cohort provided written informed consent to donate tissue for this study.

3.2. Control samples

Control samples were obtained from the bone tissue of trauma patients following a neck of femur fracture (ages 68–86, 3 women and 2 men). Exclusion criteria for control samples were the known presence of malignancy, metabolic or inflammatory disease.

3.3. Next generation sequencing

Bone and tumour tissue was homogenised under liquid nitrogen conditions using the BioPulverisor (BioSpec, Bartlesville, USA). Total RNA was extracted using the miRCURY RNA isolation kit (Exiqon, Vedbaek, Denmark) according to manufacturer's instructions. RNA concentration and integrity was measured on the NanoDrop 8000 Spectrophotometer (Thermo Fisher Scientific, Paisley, UK) and visually assessed by agarose gel electrophoresis with ethidium bromide staining. RNA was stored at − 80 °C. All libraries were constructed using 1 μg of RNA which was ligated to 3′ and 5′ HD adapters (Xu et al., 2015). Ligated RNA products were reverse transcribed to cDNA and amplified by PCR. The cDNA products expected to contain 19–33 base pair inserts were selected and purified by 8% polyacrylamide gel electrophoresis and ethanol precipitation. We performed next generation sequencing on the HiSeq 2500 Ultra-High Throughput Sequencing System (Illumina, San Diego, USA) at the Earlham Institute, Norwich Research Park.

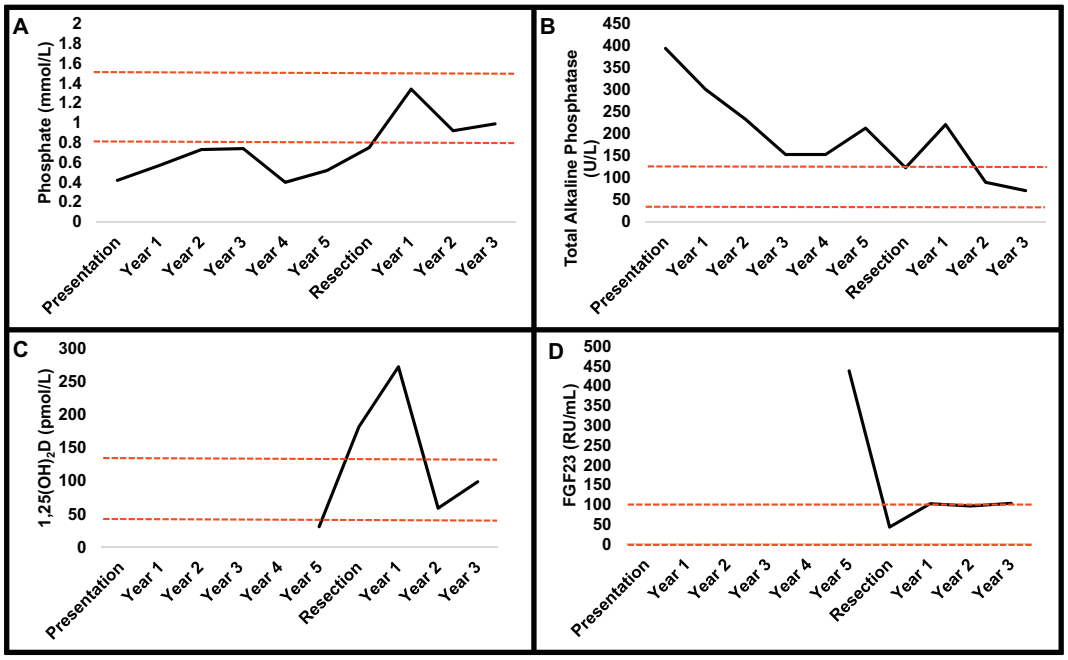

Fig. 2. Serum biochemistry performed on a patient who presented to our clinic with bone pain and muscle weakness. In the fifth year we detected $1,25(OH)_2D$ deficiency and C-Terminal FGF23 elevation which initiated the search for a PMT. A PMT was discovered and resected and the patient was followed up for three years. (A) Serum phosphate is consistently deficient until normalised by tumour resection. (B) Serum total alkaline phosphatase is significantly elevated on first presentation. Concentrations gradually declined and returned to normal two years post-resection. (C) Serum $1,25(OH)_2D$ is investigated in the fifth year and reported to be deficient. The effects of vitamin D supplementation are clearly visible post-resection when *CYP27B1* is no longer inhibited by C-Terminal FGF23 produced by the tumour. (D) Serum C-Terminal FGF23 is investigated in the fifth year and reported to be significantly elevated. Tumour resection normalises C-Terminal FGF23. C-Terminal FGF23 now remains at the upper limit of the reference range. In all figures the dotted red lines represent the upper and lower limit of the reference range. (For interpretation of the references to colour in this figure legend, the reader is referred to the web version of this article.)

3.4. Bioinformatics analysis

Raw fastq files were converted to fasta format. Reads containing unassigned nucleotides (Ns) were excluded. The 3′ HD adapter was trimmed using perfect sequence similarity to the first 8 nucleotides (nt) of the 3′ HiSeq 2500 adapter (TGGAATTC). The HD signatures from both the 5′ and 3′ ends were also trimmed (Stocks et al., 2012). Reads with low sequence complexity, i.e. with an overrepresentation of one nucleotide for > 60% of the sequence length, were excluded. As part of the quality check the size class distributions for redundant and non-redundant reads were plotted side by side with the complexity distributions (Mohorianu et al., 2011). Reads were mapped full length with no gaps or mismatches to the human genome (v38) and corresponding annotations using PatMaN (Prufer et al., 2008). The latest set of human miRNAs was downloaded from miRBase v21 (Kozomara and Griffiths-Jones, 2014). Small RNA expression levels were normalised using a scaling approach, reads per total, to a fixed total of 10 million reads (Table 2) (Mortazavi et al., 2008). As with all human studies there was variability in control samples (when compared to inbred genetic models such as mice and fruit flies where variability is minimal) so differentially expressed reads between the tumour and control samples were identified using both an expression interval approach and pair-wise comparison using offset fold change with an empirically determined offset of 20 (Mohorianu et al., 2011, 2013; Beckers et al., 2017). Comparison of the replicates was conducted using scatter plots, size-split boxplot of the replicate-to-replicate differential expression, intersection and Jaccard similarity analyses (Mohorianu et al., 2011). The analysis was conducted using custom-made Perl (5.24.0.1) and R (3.2.2) scripts.

4. Results

Matching against the human genome (v38) and corresponding annotations showed a size class distribution of the redundant reads resembling a bimodal distribution (Fig. 3A) and non-redundant reads resembling an even distribution (Fig. 3B). A bimodal distribution of

Table 1
Serum biochemistry performed on a patient who presented five years earlier with bone pain, muscle weakness, low serum phosphate and elevated total alkaline phosphatase. Now in the fifth year he presented with "explosive" bone pain on physical contact and required the use of a wheelchair because of severe muscle weakness. Serum biochemistries were repeated with further investigations performed for 25(OH)D, $1,25(OH)_2D$, FGF23, adjusted calcium, creatinine and intact parathyroid hormone. Phosphate, total alkaline phosphatase, $1,25(OH)_2D$ and C-Terminal FGF23 were abnormal (in red) leading to the suspicion of a paraneoplastic syndrome.

Analyte	Diagnostic method	Value	Reference range	Units
Phosphate	Architect 8000 (Abbott)	**0.52**	0.8–1.5	mmol/L
Total alkaline phosphatase	Architect 8000 (Abbott)	**213**	38–126	U/L
$1,25(OH)_2D$	RIA (IDS)	**31**	43–143	pmol/L
C-Terminal FGF23	ELISA (Immutopics)	**438**	<100	RU/mL
25(OH)D	LC-MS/MS	76	50–120	nmol/L
Adjusted calcium	Cobas® 6000 (Roche)	2.4	2.1–2.6	mmol/L
Creatinine	Cobas® 6000 (Roche)	88	55–125	μmol/L
Intact parathyroid hormone	Cobas® 6000 (Roche)	5.2	1.6–6.9	pmol/L

Table 2
Overview of the sequencing output for control (CTRL) and PMT libraries. We show total number of reads obtained per sample, total number of accepted reads which did not contain unassigned nucleotides, total number of non-redundant reads and overall sample complexities (C) which is defined as the ratio of non-redundant to redundant reads. We also show the percentage of genome matching reads assigned to miRNAs and tRNA fragments.

	Total reads	Accepted reads	Adapter reads	Non-redundant reads	C	Genome match (%)	miRNA match (%)	tRNA match (%)
PMT	20,4513,66	15,231,963	14,959,567	535,957	0.035	73	44	38
CTRL	26,735,842	26,711,859	17,171,584	911,323	0.057	73	28	9
CTRL	14,090,445	14,077,678	10,211,115	741,722	0.079	71	13	14
CTRL	28,948,651	28,922,976	25,836,859	800,979	0.034	80	34	31
CTRL	26,936,015	26,911,371	24,367,300	811,143	0.034	84	15	39
CTRL	35,001,366	34,969,913	33,113,846	653,789	0.020	87	5	74

redundant reads and even distribution of non-redundant reads is in line with previous human studies which use HD adapters for small RNA library construction (Sorefan et al., 2012; Green et al., 2017). The distribution of complexities shows a low complexity at 22 and 32 nt, corresponding to miRNAs and tRNA fragments. Low complexities are characterised by a small number of highly abundant sequences (Fig. 3C). Among the differentially expressed miRNAs, miR-197 was found to be upregulated compared to controls and miR-20b, miR-21, miR-144, and miR-335 were downregulated (Fig. 3D–H).

5. Discussion

We describe a patient who presented with bone pain and muscle weakness. Although his radiology was consistent with renal osteodystrophy, this diagnosis was dismissed due to his normal renal function. As his health deteriorated, later investigation revealed an FGF23-producing PMT in the left femoral head. The majority of PMT cases are associated with TIO. This case differs from conventional descriptions of TIO because of the diffuse sclerosis that affected the axial and parts of the appendicular skeleton. In other atypical cases where osteomalacia and osteosclerosis co-present it has been considered that vitamin D supplementation to treat osteomalacia may play a role in causing osteosclerosis, though our biochemical analysis shows a suppression of the active metabolite $1,25(OH)_2D$ (Edelson et al., 1993). The radiographic appearance of the trabeculae in the femoral necks is typical of osteomalacia when they are poorly defined and coarse. Later in the progression of the disease the trabeculae became more conspicuous as the sclerosis progressed. Acquired diffuse osteosclerosis can

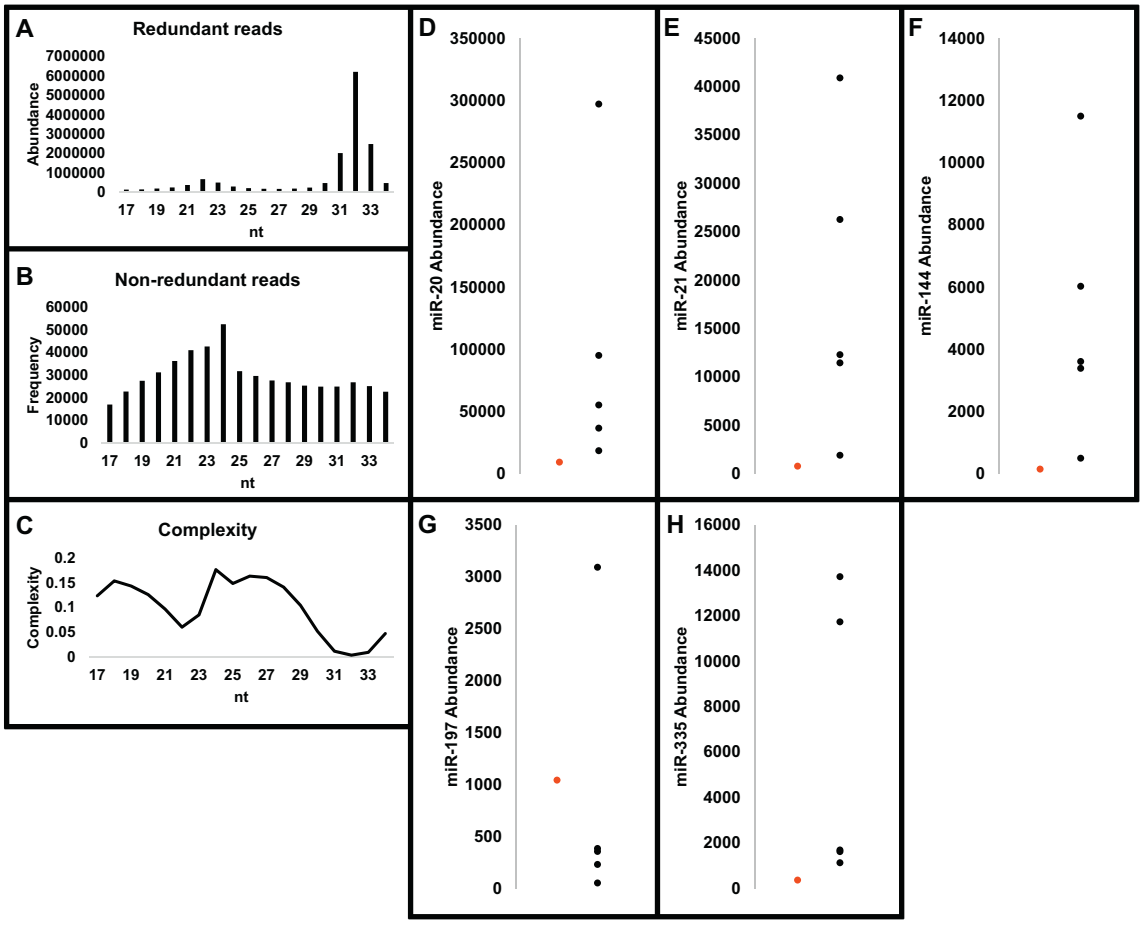

Fig. 3. Bioinformatics and sequencing analysis of next generation sequencing data. PMT size class distribution for (A) redundant reads (B) non-redundant reads (C) complexities. The size class distribution of the redundant reads is a bimodal distribution with peaks at 22 nt (miRNAs) and 32 nt (tRNA fragments). We also observe a low complexity at 22 and 32 nt (miRNAs and tRNA fragments respectively) which indicates the presence of a small number of highly abundant small RNA reads. Abundance of differentially expressed miRNAs between the tumour (in red) compared to normal samples (in black). (D) miR-20b-5p (E) miR-21-5p (F) miR-144-5p (G) miR-197-3p (H) miR-335-5p. (For interpretation of the references to colour in this figure legend, the reader is referred to the web version of this article.)

be seen in a number of conditions. In this clinical context myelofibrosis or mastocytosis might be the most important differential diagnosis with potentially similar patterns of sclerosis. Bone dysplasias such as pycnodysostosis and osteopetrosis could be excluded by the progressive nature of the condition. The slow indolent course of the disease did not fit with lymphoma, sclerotic metastases or diffuse sclerosing myeloma. The combination of osteosclerosis and osteomalacia pointed to a metabolic aetiology. While renal osteodystrophy might be the most common cause for these appearances the renal function did not support this diagnosis. In this case a less common defect in phosphate metabolism needed to be considered.

Physical examination and serum biochemistry initiated the search for a PMT. PET/CT examination identified a lesion in the left femoral head which was confirmed by biopsy as a PMT. Resection of the tumour resulted in prompt resolution of the biochemical abnormalities and rapid improvement of the patient's condition. To investigate the molecular biology of a PMT associated with osteosclerosis we performed next generation sequencing to identify differential expression of miRNAs. We found a downregulation of miR-20b, miR-144 and miR-335 (Fig. 3D–H). This miRNA signature is similar to previous observations in osteosarcoma (Wang et al., 2013, 2015; Liu et al., 2016). MiR-335 has been shown to negatively regulate translation of rho associated coiled-coil containing protein kinase 1 (*ROCK1*) (Wang et al., 2013). The role of ROCK1 is to promote cytoskeletal changes associated with cancer cell migration and metastasis. MiR-20b has been shown to negatively regulate translation of *HIF1A* and inhibit the proliferation and migration of osteosarcoma cells (Liu et al., 2016). Upregulation of HIF1A has previously been linked to sarcoma metastasis (El-Naggar et al., 2015). We also found a downregulation of miR-21 which is one of the most frequently upregulated miRNAs in cancer. MiR-21 acts by suppressing the translation of phosphatases which normally inhibit the activity of protein kinase B (PKB) and mitogen-activated protein kinases (MAPK) signalling (Musilova and Mraz, 2015). We speculate that miR-21 downregulation in this case may underlie the apparently benign phenotype despite the osteosarcoma miRNA profile.

We used TargetScan v7.1 to identify targets of miR-197 which we observe to be upregulated. *FGF23* transcript was identified as a predicted target for canonical seed region matching and silencing by miR-197. The cellular transcriptome is a dynamic set of transcripts which is able to respond to endogenous and exogenous signals (Green et al., 2016). Our finding of an upregulated miRNA to target a hypoxia induced transcript, *FGF23*, is supportive of a previous prediction that increased transcriptional plasticity and negative regulation of ectopically expressed genes may act as an innate cellular defence mechanism in order to maintain genomic homeostasis (Green et al., 2016).

PMT was first used in 1987 as an umbrella term to comprise the diverse mesenchymal lesions that lead to phosphate wasting. The majority of PMTs (> 80%) are mixed connective tissue variants which consist of sheets of primitive stromal cells with small nuclei interposed with a proliferating vascular component containing giant cells and multiple foci of immature cartilage, osteoid and bone (Shane et al., 1997). It will be important to perform further research into miRNA profiles in other PMTs to observe if differences exist in such tumours or if there is consistency in the profile that could be used as a diagnostic/prognostic tool. Our findings should be compared with future PMT cases that result in non-sclerotic type lesions. The patient described in this report was investigated for five years before an underlying tumour was considered, located and resected, demonstrating the difficulty that can exist in making the diagnosis early in the disease. In future it may be possible to examine circulating cells or molecules to look at a profile of markers to help confirm the molecular diagnosis.

Data availability

The sequencing data presented in this study is publicly available on Gene Expression Omnibus (GEO) under the accession GSE97957.

Disclosures

No conflict to declare.

Acknowledgements

This work was supported by Big C (14-08R). We thank the Supra-Regional Assay Service for Bone Markers (Bioanalytical Facility, Norwich Medical School and Department of Clinical Biochemistry, Norfolk and Norwich University Hospital). We are very grateful to the patient.

References

Beckers, M.L., Mohorianu, I., Stocks, M.B., Applegate, C., Dalmay, T., Moulton, V., 2017. Comprehensive processing of high throughput small RNA sequencing data including quality checking, normalization and differential expression analysis using the UEA sRNA Workbench. RNA. http://dx.doi.org/10.1261/rna.059360.116.

Berndt, T., Kumar, R., 2007. Phosphatonins and the regulation of phosphate homeostasis. Annu. Rev. Physiol. 69, 341–359. http://dx.doi.org/10.1146/annurev.physiol.69.040705.141729.

Blondal, T., Nielsen, S.J., Baker, A., Andreasen, D., Mouritzen, P., Teilum, M.W., Dahlsveen, I.K., 2013. Assessing sample and miRNA profile quality in serum and plasma or other biofluids. Methods 59 (1), S1–6. http://dx.doi.org/10.1016/j.ymeth.2012.09.015.

Chong, W.H., Molinolo, A.A., Chen, C.C., Collins, M.T., 2011. Tumor-induced osteomalacia. Endocr. Relat. Cancer 18 (3), R53–77. http://dx.doi.org/10.1530/erc-11-0006.

Edelson, G.W., Shih, M.S., Parfitt, A.M., 1993. A unique case of adult hypophosphatemic osteomalacia. Bone 14 (5), 707–710.

El-Naggar, A.M., Veinotte, C.J., Cheng, H., Grunewald, T.G., Negri, G.L., Somasekharan, S.P., Corkery, D.P., Tirode, F., Mathers, J., Khan, D., et al., 2015. Translational activation of HIF1alpha by YB-1 promotes sarcoma metastasis. Cancer Cell 27 (5), 682–697. http://dx.doi.org/10.1016/j.ccell.2015.04.003.

Goldblum, J.R., Weiss, S.W., Folpe, A.L., 2013. Enzinger and Weiss's Soft Tissue Tumors, 6th ed. Saunders.

Green, D., Dalmay, T., Chapman, T., 2016. Microguards and micromessengers of the genome. Heredity 116 (2), 125–134.

Green, D., Mohorianu, I., McNamara, I., Dalmay, T., Fraser, W.D., 2017. miR-16 is highly expressed in Paget's associated osteosarcoma. Endocr. Relat. Cancer 24 (5), L27–l31. http://dx.doi.org/10.1530/erc-16-0487.

Kozomara, A., Griffiths-Jones, S., 2014. miRBase: annotating high confidence microRNAs using deep sequencing data. Nucleic Acids Res. 42 (Database issue), D68–73. http://dx.doi.org/10.1093/nar/gkt1181.

Lee, J.C., Jeng, Y.M., Su, S.Y., Wu, C.T., Tsai, K.S., Lee, C.H., Lin, C.Y., Carter, J.M., Huang, J.W., Chen, S.H., et al., 2015. Identification of a novel FN1-FGFR1 genetic fusion as a frequent event in phosphaturic mesenchymal tumour. J. Pathol. 235 (4), 539–545. http://dx.doi.org/10.1002/path.4465.

Liu, M., Wang, D., Li, N., 2016. MicroRNA-20b downregulates HIF-1alpha and inhibits the proliferation and invasion of osteosarcoma cells. Oncol. Res. 23 (5), 257–266. http://dx.doi.org/10.3727/096504016x14562725373752.

Mohorianu, I., Schwach, F., Jing, R., Lopez-Gomollon, S., Moxon, S., Szittya, G., Sorefan, K., Moulton, V., Dalmay, T., 2011. Profiling of short RNAs during fleshy fruit development reveals stage-specific sRNAome expression patterns. Plant J. 67 (2), 232–246. http://dx.doi.org/10.1111/j.1365-313X.2011.04586.x.

Mohorianu, I., Stocks, M.B., Wood, J., Dalmay, T., Moulton, V., 2013. CoLIde: a bioinformatics tool for CO-expression-based small RNA loci identification using high-throughput sequencing data. RNA Biol. 10 (7), 1221–1230. http://dx.doi.org/10.4161/rna.25538.

Mortazavi, A., Williams, B.A., McCue, K., Schaeffer, L., Wold, B., 2008. Mapping and quantifying mammalian transcriptomes by RNA-Seq. Nat. Methods 5 (7), 621–628. http://dx.doi.org/10.1038/nmeth.1226.

Musilova, K., Mraz, M., 2015. MicroRNAs in B-cell lymphomas: how a complex biology gets more complex. Leukemia 29 (5), 1004–1017. http://dx.doi.org/10.1038/leu.2014.351.

Prufer, K., Stenzel, U., Dannemann, M., Green, R.E., Lachmann, M., Kelso, J., 2008. PatMaN: rapid alignment of short sequences to large databases. Bioinformatics 24 (13), 1530–1531. http://dx.doi.org/10.1093/bioinformatics/btn223.

Rosenfeld, N., Aharonov, R., Meiri, E., Rosenwald, S., Spector, Y., Zepeniuk, M., Benjamin, H., Shabes, N., Tabak, S., Levy, A., et al., 2008. MicroRNAs accurately identify cancer tissue origin. Nat. Biotechnol. 26 (4), 462–469. http://dx.doi.org/10.1038/nbt1392.

Schetter, A.J., Leung, S.Y., Sohn, J.J., Zanetti, K.A., Bowman, E.D., Yanaihara, N., Yuen, S.T., Chan, T.L., Kwong, D.L., Au, G.K., et al., 2008. MicroRNA expression profiles associated with prognosis and therapeutic outcome in colon adenocarcinoma. JAMA 299 (4), 425–436. http://dx.doi.org/10.1001/jama.299.4.425.

Shane, E., Parisien, M., Henderson, J.E., Dempster, D.W., Feldman, F., Hardy, M.A., Tohme, J.F., Karaplis, A.C., Clemens, T.L., 1997. Tumor-induced osteomalacia: clinical and basic studies. J. Bone Miner. Res. Off. J. Am. Soc. Bone Miner. Res. 12 (9), 1502–1511. http://dx.doi.org/10.1359/jbmr.1997.12.9.1502.

Sorefan, K., Pais, H., Hall, A.E., Kozomara, A., Griffiths-Jones, S., Moulton, V., Dalmay, T., 2012. Reducing ligation bias of small RNAs in libraries for next generation

sequencing. Silence 3 (1), 4. http://dx.doi.org/10.1186/1758-907X-3-4.
Stocks, M.B., Moxon, S., Mapleson, D., Woolfenden, H.C., Mohorianu, I., Folkes, L., Schwach, F., Dalmay, T., Moulton, V., 2012. The UEA sRNA workbench: a suite of tools for analysing and visualizing next generation sequencing microRNA and small RNA datasets. Bioinformatics 28 (15), 2059–2061. http://dx.doi.org/10.1093/bioinformatics/bts311.
Thienpont, B., Steinbacher, J., Zhao, H., D'Anna, F., Kuchnio, A., Ploumakis, A., Ghesquiere, B., Van Dyck, L., Boeckx, B., Schoonjans, L., et al., 2016. Tumour hypoxia causes DNA hypermethylation by reducing TET activity. Nature. http://dx.doi.org/10.1038/nature19081.
Wang, Y., Zhao, W., Fu, Q., 2013. miR-335 suppresses migration and invasion by targeting ROCK1 in osteosarcoma cells. Mol. Cell. Biochem. 384 (1–2), 105–111. http://dx.doi.org/10.1007/s11010-013-1786-4.
Wang, W., Zhou, X., Wei, M., 2015. MicroRNA-144 suppresses osteosarcoma growth and metastasis by targeting ROCK1 and ROCK2. Oncotarget 6 (12), 10297–10308. http://dx.doi.org/10.18632/oncotarget.3305.
Xu, P., Billmeier, M., Mohorianu, I., Green, D., Fraser, W., Dalmay, T., 2015. An improved protocol for small RNA library construction using high definition adapters. Methods Next Gener. Seq. 2 (1), 1–10. http://dx.doi.org/10.1515/mngs-2015-0001.
Yanaihara, N., Caplen, N., Bowman, E., Seike, M., Kumamoto, K., Yi, M., Stephens, R.M., Okamoto, A., Yokota, J., Tanaka, T., et al., 2006. Unique microRNA molecular profiles in lung cancer diagnosis and prognosis. Cancer Cell 9 (3), 189–198. http://dx.doi.org/10.1016/j.ccr.2006.01.025.
Zhang, Q., Doucet, M., Tomlinson, R.E., Han, X., Quarles, L.D., Collins, M.T., Clemens, T.L., 2016. The hypoxia-inducible factor-1alpha activates ectopic production of fibroblast growth factor 23 in tumor-induced osteomalacia. Bone Res. 4, 16011. http://dx.doi.org/10.1038/boneres.2016.11.